NASA TECHNICAL NOTE

NASA TN D-2655

NASA TN D-2655

TRIM REQUIREMENTS AND STATIC-STABILITY DERIVATIVES FROM A WIND-TUNNEL INVESTIGATION OF A LIFTING ROTOR IN TRANSITION

by Julian L. Jenkins, Jr.

Langley Research Center

Langley Station, Hampton, Va.

NATIONAL AERONAUTICS AND SPACE ADMINISTRATION • WASHINGTON, D. C. • FEBRUARY 1965

NASA TN-D-2655

TRIM REQUIREMENTS AND STATIC-STABILITY DERIVATIVES FROM A WIND-TUNNEL INVESTIGATION OF A LIFTING ROTOR IN TRANSITION

By Julian L. Jenkins, Jr.

Langley Research Center
Langley Station, Hampton, Va.

NATIONAL AERONAUTICS AND SPACE ADMINISTRATION

For sale by the Office of Technical Services, Department of Commerce,
Washington, D.C. 20230 -- Price $2.00

TRIM REQUIREMENTS AND STATIC-STABILITY DERIVATIVES FROM A WIND-TUNNEL INVESTIGATION OF A LIFTING ROTOR IN TRANSITION

By Julian L. Jenkins, Jr.
Langley Research Center

SUMMARY

16892

A wind-tunnel investigation of a 15-foot-diameter rotor was made to determine the trim requirements and static-stability derivatives for rotor operation at transition speeds. In addition, photographs of a vertical tuft grid in the longitudinal plane below the rotor were taken to indicate the influence of the rotor downwash on an aircraft fuselage.

The linear increase in longitudinal control requirement with increasing speed exhibited by the rotor suggests that the longitudinal control-position instability encountered at low speeds may be primarily a function of rotor-fuselage interference effects. The comparisons of experimental with theoretical static-stability derivatives indicate that the derivatives of rotor thrust, torque, and longitudinal flapping are predictable at tip-speed ratios as low as 0.04.

AUTHOR

INTRODUCTION

The rapid change in the amount and character of induced flow associated with the transition of rotary-wing aircraft through the speed range of approximately 15 to 50 knots can produce large changes in the rotor and fuselage trim requirements. These changes in trim, which often include ranges of cyclic control-position instability with speed, tend to make precision flight difficult. Although precision control in the transition speed range is generally of secondary interest in visual flight, during instrument approaches (as would be required for all-weather flight), the pilot may be required to hold a precise speed for several minutes. Thus, design of an all-weather rotary-wing aircraft requires a thorough understanding of rotor parameters throughout the transition speed range.

As part of a broad research effort concerning the all-weather capability of rotary-wing aircraft, wind-tunnel tests of a 15-foot-diameter rotor were conducted in the Langley full-scale tunnel to determine rotor trim requirements and static-stability derivatives at transition speeds. Of particular interest

is the longitudinal trim requirement since it has required special treatment, owing to control-position instabilities with speed, in the flying qualities criteria. (See ref. 1.)

The present investigation was conducted with a two-blade teetering rotor operating at an initial rotor lift coefficient of approximately 0.0045 for a range of rotor disk angles of attack from 10.5° to -24.5°. Measurements included rotor forces, torque, and blade flapping and feathering motions for independent changes in tunnel velocity, collective pitch, and shaft angle of attack. In addition, photographs of a vertical tuft grid located in the longitudinal plane below the rotor are presented to indicate the possible influence of the rotor wake on an aircraft fuselage and trim surfaces.

Calculations that include the effect of a longitudinal variation of rotor induced flow are compared with measured results to indicate the predictability of the static-stability derivatives. The equations used to compute the derivatives were based on rotor blade-element theory.

SYMBOLS

The direction of positive forces and angles is shown in figure 1.

A_o collective pitch angle; angle between line of zero lift of blade section and plane perpendicular to axis of no feathering, radians unless otherwise noted

a slope of curve of section lift coefficient against section angle of attack, per radian

a' angle between control axis and resultant-force vector, radians unless otherwise noted

a_1 first-harmonic longitudinal flapping angle, radians unless otherwise noted

b number of blades

b_1 first-harmonic lateral flapping angle, radians unless otherwise noted

c blade section chord, ft

$\bar{c}_{d,o}$ mean profile drag coefficient

C_H rotor drag (H-force) coefficient, $\frac{H}{\rho\pi R^2(\Omega R)^2}$

$C_{L,R}$ rotor lift coefficient, $\frac{L}{\rho\pi R^2(\Omega R)^2}$

C_Q rotor torque coefficient, $\frac{Q}{\rho\pi R^2(\Omega R)^2 R}$

C_R rotor resultant-force coefficient, $\left(C_T^2 + C_H^2\right)^{1/2}$

C_T rotor thrust coefficient, $\frac{T}{\rho\pi R^2(\Omega R)^2}$

H longitudinal component of rotor resultant force perpendicular to shaft axis, lb

I_h mass moment of inertia of blade about flapping hinge, slug-ft^2

L rotor lift, lb

Q rotor torque, ft-lb

R rotor radius, ft

T rotor thrust along the shaft axis, lb

V free-stream velocity, ft/sec

v induced inflow velocity at rotor, ft/sec

v_l rate of change of induced velocity along fore-and-aft diameter of rotor, $v \tan \frac{\chi}{2}$, ft/sec

α control-axis angle of attack, radians

α_s rotor shaft angle of attack, radians

γ mass constant of rotor blade (blade Lock number), $\frac{\rho a c R^4}{I_h}$

λ rotor inflow ratio, $\frac{V \sin \alpha - v}{\Omega R}$

λ' rotor inflow variation parameter, $\frac{v_l}{\Omega R}$

μ rotor tip-speed ratio, $\frac{V \cos \alpha}{\Omega R}$

ρ mass density of air, slugs/cu ft

σ rotor solidity, $\frac{bc}{\pi R}$

χ wake skew angle, $\tan^{-1}\left(\frac{-\mu}{\lambda}\right) + a_1$, radians

Ω rotor angular velocity, radians/sec

APPARATUS

The rotor installed in the Langley full-scale tunnel is shown in figure 2. The rotor had a diameter of 15.00 feet, a constant blade chord of 0.64 foot, and a corresponding solidity σ of 0.0543. The blades were untwisted NACA 0012 airfoil sections and had a Lock number γ of 4.85. Rotor thrust and torque were measured with strain-gage instrumentation located in the rotor support tower. (See fig. 3.) This apparatus automatically corrected for thrust loads carried by the blade pitch-rods and for the frictional torque of the swash plate.

Blade flapping and feathering motions were sensed by strain gages and recorded on an oscillograph. A Fourier analysis was performed on these data to obtain flapping and feathering coefficients. The impulse from a 24-cycle signal generator was recorded on an oscillograph and used to determine rotational speed and blade azimuth position.

A large ground-reflection plane was installed approximately 14 feet below the rotor to minimize the problem of wind-tunnel jet-boundary corrections. The resulting corrections are discussed in the following section.

TESTS AND CORRECTIONS

The tests were conducted at a tip speed of approximately 465 fps, which corresponds, in hovering, to a tip Reynolds number of 1.89×10^6.

The procedure employed to obtain the static-stability derivatives was to trim the rotor disk normal to the shaft for a given shaft attitude and tunnel velocity at a rotor lift coefficient of approximately 0.0045. From these initial trim settings, small, independent changes in collective pitch, shaft angle, and tunnel velocity were made and the resulting data recorded. These measurements were plotted against the independent variables and the slope through the trim point determined. The derivatives were obtained at rotor angles of attack of 10.5°, -4.5°, -14.5°, and -24.5° for tip-speed ratios from approximately 0.04 to 0.17.

The data have been corrected for hub and fuselage tares. A stream-angle correction of 0.5° to angle of attack was also included.

Jet-boundary corrections have been applied according to the procedure outlined in reference 2 to obtain free-stream conditions. Generally, these corrections were small (less than 1° angle of attack and 1.5 fps velocity), except

for the lowest speeds at 10.5° and -4.5° where the angle-of-attack corrections were 3.6° and 1.4°, respectively. In order to obtain corrected data at constant angles of attack, estimates of the jet-boundary corrections made prior to the tests were used to set the rotor attitude at such an angle that when the measured data were corrected, the desired rotor attitude was attained.

The overall accuracies of the data are believed to be within the following limits:

C_T	±0.00006
C_H	±0.00003
C_Q	±0.00001
Rotor tip speed, fps	±1
Flapping and feathering angles, deg	±0.25

CALCULATED STABILITY DERIVATIVES

The equations used to calculate the static-stability derivatives are based on the simple blade-element theory described in reference 3. Two significant modifications should be noted. First, the equations include a term to account for a linear, longitudinal variation in inflow. (See ref. 4.) Second, the flapping coefficients were determined by summing moments for a teetering rotor as described in reference 5. This summation results in equations for the lateral flapping b_1 and its derivatives that are functions of the longitudinal inflow parameter λ'. The equations are presented in the appendix without development inasmuch as the development parallels the procedure described in reference 6.

The procedure followed in calculating the derivatives was to use the measured blade collective pitch A_o, the control-axis angle of attack α, and the tip-speed ratio μ and to vary the inflow ratio λ until the calculated control-axis angle equaled the measured angle. With the inflow ratio determined, the derivatives were then computed. A constant lift-curve slope ($a = 5.55$ per radian) and a mean profile drag coefficient $\left(\bar{c}_{d,o} = 0.01\right)$ were used for all calculations.

Since the equations for the thrust and in-plane force and their respective derivatives are referenced to the control axis, these derivatives have been transferred to the shaft axis for comparison with the experimental derivatives.

RESULTS AND DISCUSSION

A summary of the rotor characteristics for rotor tip-path-plane angles of attack of approximately 10.5°, -4.5°, -14.5°, and -24.5° is presented in figure 4. These data are averaged values of the individual coefficients and angles for all similar trim settings of the tests. Since fuselage aerodynamics

and accelerations and type of rotor operation (pure helicopter or tilt rotor) fix the rotor attitude, these data at constant rotor attitude over the range of tip-speed ratios do not represent exact conditions of transition flight. However, the range of angles should be sufficient to indicate notable effects for both pure-helicopter and tilt-rotor operations.

The large changes in rotor torque with speed indicated in figure 4 illustrate one of the problems associated with the transition. Such changes can significantly affect the pilot's ability to perform precision maneuvers during low-speed instrument flight. For example, when operating on the back side of the power-required curve at a rotor angle of -4.5° (an approximate, pure-helicopter attitude), the 30-percent reduction in the torque coefficient from a tip-speed ratio of 0.04 to 0.17 indicates a change in directional control for most helicopters as well as a change in collective pitch.

Flight tests have indicated that cyclic control-position instability with speed can occur during transition. (See, for example, refs. 7 and 8.) However, the longitudinal trim curves, the variation of a' with $V/\Omega R$ presented in figure 4, do not indicate any trend for a control-position instability at nose-down attitudes. In fact, the curves increase almost linearly with tip-speed ratio for the range covered. This result suggests that longitudinal control-position instability may be due primarily to the effects of aerodynamic wake interference on the fuselage and trim surfaces and therefore would be highly dependent on the particular aircraft configuration.

The lateral trim, as denoted in figure 4 by the lateral flapping b_1, shows a trend indicating a control-position nonlinearity. This nonlinearity is believed to be a function of the longitudinal variation of inflow. Calculations in which a linear, longitudinal inflow variation was considered, accounted for approximately 50 to 60 percent of the measured cyclic values of lateral flapping. The calculations also indicated nonlinearities in lateral flapping for the range of rotor attitudes and tip-speed ratios covered in this investigation. The remaining discrepancy is believed to be due, in part, to coning caused by blade bending, inasmuch as this coning also contributes to the lateral flapping of a teetering rotor.

Static-Stability Derivatives

Rotor static-stability derivatives with respect to collective pitch A_0, angle of attack α, and $V/\Omega R$ are presented in figures 5 to 7, respectively. The experimental derivatives are compared with derivatives calculated from the equations included in the appendix. A discussion of the relative importance of the stability derivatives is presented in reference 9.

Although the theoretical derivatives presented are based on equations which include numerous simplifying assumptions, the agreement between experiment and theory for the C_T derivatives is very good and that for the C_Q and a_1 derivatives appears, in general, to be acceptable for tip-speed ratios as low as 0.04. The other derivatives (C_H, b_1, and a') do not show good agreement; however, the inconsistencies that exist between the experimental and theoretical

in-plane force (C_H) derivatives can be attributed, in part, to experimental error in measuring the small in-plane forces from which the derivatives were obtained. Since the angle between the control axis and the resultant-force vector a' is a direct function of the in-plane force, derivatives of a' are also dependent on the accuracy of in-plane force measurements. The assumption of a constant profile drag coefficient in the calculations would also cause both the torque and in-plane force derivatives to be underestimated and would have a more significant effect on the derivatives with respect to collective pitch than on derivatives with respect to angle of attack or velocity since the mean blade-section angle of attack increases rapidly with increases in collective pitch.

The discrepancies which exist between the experimental and theoretical lateral flapping b_1 derivatives are primarily in magnitude rather than trends and can arise from two sources. First, coning of the rotor due to blade bending may affect the lateral flapping derivative; and, second, underestimation of the linear, induced inflow variation could cause the lateral flapping derivatives to be underestimated, as is generally the case for the derivatives presented in figures 5 to 7.

In order to evaluate blade bending effects, the lateral flapping derivatives were calculated for a free-to-cone rotor (including induced inflow variation) and are presented in figures 5 to 7. Although, in most cases, these calculations are in better agreement with the measured results than are those for the teetering rotor, these calculations are believed to be representative of an upper limit for the lateral flapping derivative of a teetering rotor with blade bending considered. Since the bending effects on lateral flapping thus cannot fully account for the discrepancies between the experimental and theoretical derivatives, it appears that the inflow variation parameter λ' is underestimated. In fact, as illustrated in reference 10, the inflow variation in the longitudinal plane is not linear and the areas near the leading and trailing edge of the rotor disk show an inflow variation with a direction and magnitude which could produce the type of discrepancies noted herein.

Tuft-Grid Photographs

Photographs of a vertical tuft grid parallel to the longitudinal axis, approximately 2 feet to the right of center, and below the rotor to indicate the influence of the rotor downwash on an aircraft fuselage are presented in figures 8 and 9. Although data were not taken at tip-speed ratios less than 0.043, photographs of the flow field at a tip-speed ratio of approximately 0.032 are presented. The rotor wakes at this low tip-speed ratio appear to have essentially the same pattern for all six attitudes. (See, for example, fig. 8.) There is a definite rolling up of the wake at the leading edge of the rotor which is similar to that produced by hovering in ground effect. As speed increases, this rollup moves downstream and has essentially disappeared at a tip-speed ratio of 0.08. (See fig. 9.)

This rapid transition of the rotor wake from a nearly vertical pattern (hovering) to a more horizontal pattern could seriously affect fuselage and

trim-surface aerodynamics. The problem of rotor-fuselage interference, however, is complex, and conseqeuntly an evaluation of interference effects at low speeds will be highly dependent on aircraft configuration.

CONCLUDING REMARKS

Trim requirements and static-stability derivatives have been determined for a 15-foot-diameter lifting rotor operating at transition speeds. The longitudinal trim measurements exhibited an almost linear increase with increasing speed. This linearity infers that the longitudinal cyclic control-position instability sometimes encountered by helicopters at low speed may be primarily a function of rotor-fuselage interference effects. Also, the tuft photographs indicate a rapid transition of the rotor wake from a nearly vertical pattern to a more horizontal pattern that could seriously affect fuselage and trim-surface aerodynamics.

The comparisons of experimental with theoretical static-stability derivatives indicate that the derivatives of rotor thrust, torque, and longitudinal flapping are predictable at tip-speed ratios as low as 0.04.

Langley Research Center,
National Aeronautics and Space Administration,
Langley Station, Hampton, Va., November 13, 1964.

APPENDIX

SUMMARY OF EQUATIONS FOR COMPUTING STABILITY DERIVATIVES FOR A TEETERING ROTOR

The equations presented are based on the simple blade-element theory described in reference 3; however, a term to account for a linear, longitudinal variation in inflow has been added.

Derivatives of Average Induced Velocity

The equations for computing the derivatives of the average induced velocity with respect to collective pitch, angle of attack, and velocity are

$$\frac{\partial v}{\partial A_o} = \frac{\frac{\sigma a}{8}\left(\frac{2}{3} + \mu^2\right)}{\frac{\left(\mu^2 + \lambda^2\right)^{1/2}}{\Omega R} - \frac{v\lambda}{(\Omega R)^2\left(\mu^2 + \lambda^2\right)^{1/2}} + \frac{\sigma a}{8\Omega R}} \tag{1a}$$

$$\frac{\partial v}{\partial \alpha} = \frac{\mu\left[\frac{v^2}{(\Omega R)^2\left(\mu^2 + \lambda^2\right)^{1/2}} + \frac{\sigma a}{8}\left(1 - 2A_o\mu \tan \alpha\right)\right]}{\frac{\left(\mu^2 + \lambda^2\right)^{1/2}}{\Omega R} - \frac{v\lambda}{(\Omega R)^2\left(\mu^2 + \lambda^2\right)^{1/2}} + \frac{\sigma a}{8\Omega R}} \tag{1b}$$

$$\frac{\partial v}{\partial V} = \frac{\frac{\sigma a}{8}\left(2A_o\mu \cos \alpha + \sin \alpha\right) - \frac{v(V - v \sin \alpha)}{(\Omega R)^2\left(\mu^2 + \lambda^2\right)^{1/2}}}{\left(\mu^2 + \lambda^2\right)^{1/2} - \frac{v\lambda}{\Omega R\left(\mu^2 + \lambda^2\right)^{1/2}} + \frac{\sigma a}{8}} \tag{1c}$$

APPENDIX

Derivatives of Longitudinal Induced Velocity

The equations for computing the derivatives of the linear, longitudinal induced velocity with respect to collective pitch, angle of attack, and velocity are

$$\frac{\partial v_1}{\partial A_0} = \frac{\partial v}{\partial A_0} \tan \frac{\chi}{2} + \frac{v}{1 + \cos \chi}\left[\frac{\frac{8}{3}\mu}{1 - \frac{1}{2}\mu^2} - \left(\frac{1}{\mu^2 + \lambda^2} + \frac{2}{1 - \frac{1}{2}\mu^2}\right)\frac{\mu}{\Omega R}\frac{\partial v}{\partial A_0}\right] \tag{2a}$$

$$\frac{\partial v_1}{\partial \alpha} = \frac{\partial v}{\partial \alpha} \tan \frac{\chi}{2} + \frac{v}{1 + \cos \chi}\left[\frac{V^2 - Vv \sin \alpha}{(\Omega R)^2\left(\mu^2 + \lambda^2\right)} + \frac{2\mu^2}{1 - \frac{1}{2}\mu^2} - \frac{1 + \frac{1}{2}\mu^2}{1 - \frac{1}{2}\mu^2} a_1 \tan \alpha\right.$$

$$\left. - \left(\frac{1}{\mu^2 + \lambda^2} + \frac{2}{1 - \frac{1}{2}\mu^2}\right)\frac{\mu}{\Omega R}\frac{\partial v}{\partial \alpha}\right] \tag{2b}$$

$$\frac{\partial v_1}{\partial V} = \frac{\partial v}{\partial V} \tan \frac{\chi}{2} + \frac{v}{1 + \cos \chi}\left[\frac{v \cos \alpha}{(\Omega R)^2\left(\mu^2 + \lambda^2\right)} + \frac{1 + \frac{1}{2}\mu^2}{1 - \frac{1}{2}\mu^2}\frac{a_1 \cos \alpha}{\mu \Omega R}\right.$$

$$\left. + \frac{2\mu \sin \alpha}{\left(1 - \frac{1}{2}\mu^2\right)\Omega R} - \left(\frac{1}{\mu^2 + \lambda^2} + \frac{2}{1 - \frac{1}{2}\mu^2}\right)\frac{\mu}{\Omega R}\frac{\partial v}{\partial V}\right] \tag{2c}$$

Derivatives of First-Harmonic Longitudinal Flapping Coefficient

The equations for computing the derivatives of the first-harmonic longitudinal flapping coefficient with respect to collective pitch, angle of attack, and $V/\Omega R$ are

$$\frac{\partial a_1}{\partial A_0} = \frac{2\mu\left(\frac{4}{3}\Omega R - \frac{\partial v}{\partial A_0}\right)}{\Omega R\left(1 - \frac{1}{2}\mu^2\right)} \tag{3a}$$

$$\frac{\partial a_1}{\partial \alpha} = \frac{2\mu}{1 - \frac{1}{2}\mu^2}\left(\mu - \frac{1}{\Omega R}\frac{\partial v}{\partial \alpha}\right) - a_1 \frac{1 + \frac{1}{2}\mu^2}{1 - \frac{1}{2}\mu^2} \tan \alpha \tag{3b}$$

$$\frac{\partial a_1}{\partial\left(\frac{V}{\Omega R}\right)} = a_1 \frac{1 + \frac{1}{2}\mu^2}{\mu\left(1 - \frac{1}{2}\mu^2\right)} \cos \alpha + \frac{2\mu}{1 - \frac{1}{2}\mu^2}\left(\sin \alpha - \frac{\partial v}{\partial V}\right) \tag{3c}$$

APPENDIX

Derivatives of First-Harmonic Lateral Flapping Coefficient

The equations for computing the derivatives of the first-harmonic lateral flapping coefficient with respect to collective pitch, angle of attack, and $V/\Omega R$ are

$$\frac{\partial b_1}{\partial A_0} = \frac{1}{\Omega R\left(1 + \frac{1}{2}\mu^2\right)} \frac{\partial v_1}{\partial A_0} \tag{4a}$$

$$\frac{\partial b_1}{\partial \alpha} = \frac{1}{\Omega R\left(1 + \frac{1}{2}\mu^2\right)} \frac{\partial v_1}{\partial \alpha} + \frac{b_1 \mu^2 \tan \alpha}{1 + \frac{1}{2}\mu^2} \tag{4b}$$

$$\frac{\partial b_1}{\partial\left(\frac{V}{\Omega R}\right)} = \frac{1}{1 + \frac{1}{2}\mu^2} \frac{\partial v_1}{\partial V} - \frac{b_1 \mu \cos \alpha}{1 + \frac{1}{2}\mu^2} \tag{4c}$$

Derivatives of Rotor Thrust Coefficient

The equations for computing the derivatives of the rotor thrust coefficient with respect to collective pitch, angle of attack, and $V/\Omega R$ are

$$\frac{\partial C_T}{\partial A_0} = \frac{\sigma a}{4}\left(\frac{2}{3} + \mu^2 - \frac{1}{\Omega R} \frac{\partial v}{\partial A_0}\right) \tag{5a}$$

$$\frac{\partial C_T}{\partial \alpha} = \frac{\sigma a}{4}\left(\mu - 2A_0 \mu^2 \tan \alpha - \frac{1}{\Omega R} \frac{\partial v}{\partial \alpha}\right) \tag{5b}$$

$$\frac{\partial C_T}{\partial\left(\frac{V}{\Omega R}\right)} = \frac{\sigma a}{4}\left(2A_0 \mu \cos \alpha + \sin \alpha - \frac{\partial v}{\partial V}\right) \tag{5c}$$

APPENDIX

Derivatives of Rotor Drag-Force Coefficient

The equations for computing the derivatives of the rotor drag-force coefficient with respect to collective pitch, angle of attack, and $V/\Omega R$ are

$$\frac{\partial C_H}{\partial A_o} = \frac{\sigma a}{4}\left[\frac{2}{3}a_1 - \mu\lambda + \frac{\partial v}{\partial A_o}\left(A_o\frac{\mu}{\Omega R} - \frac{3}{2}\frac{a_1}{\Omega R}\right) + \frac{\partial a_1}{\partial A_o}\left(\frac{3}{2}\lambda + a_1\mu + \frac{2}{3}A_o\right)\right.$$

$$\left. + \frac{\partial b_1}{\partial A_o}\frac{\mu\lambda'}{8} + \frac{\partial v_1}{\partial A_o}\frac{b_1\mu}{8\Omega R}\right] \tag{6a}$$

$$\frac{\partial C_H}{\partial \alpha} = \frac{\sigma a}{4}\left[\mu\left(A_o\lambda - \frac{\bar{c}_{d,o}}{a} - \frac{1}{2}a_1^2 - \frac{1}{8}b_1\lambda'\right)\tan\alpha - A_o\mu^2 + \frac{3}{2}a_1\mu + \frac{1}{\Omega R}\frac{\partial v}{\partial \alpha}\left(A_o\mu - \frac{3}{2}a_1\right)\right.$$

$$\left. + \frac{\partial a_1}{\partial \alpha}\left(\frac{2}{3}A_o + \frac{3}{2}\lambda + a_1\mu\right) + \frac{\partial b_1}{\partial \alpha}\frac{\mu\lambda'}{8} + \frac{\partial v_1}{\partial \alpha}\frac{b_1\mu}{8\Omega R}\right] \tag{6b}$$

$$\frac{\partial C_H}{\partial\left(\frac{V}{\Omega R}\right)} = \frac{\sigma a}{4}\left[\frac{\bar{c}_{d,o}}{a}\cos\alpha - A_o\left(\lambda\cos\alpha + \mu\sin\alpha\right) + \frac{3}{2}a_1\sin\alpha\right.$$

$$+ \frac{1}{2}a_1^2\cos\alpha + \frac{1}{8}b_1\lambda'\cos\alpha + \frac{\partial v}{\partial V}\left(A_o\mu - \frac{3}{2}a_1\right)$$

$$\left. + \frac{\partial a_1}{\partial\left(\frac{V}{\Omega R}\right)}\left(\frac{2}{3}A_o + \frac{3}{2}\lambda + a_1\mu\right) + \frac{\partial b_1}{\partial\left(\frac{V}{\Omega R}\right)}\frac{\mu\lambda'}{8} + \frac{\partial v_1}{\partial V}\frac{b_1\mu}{8}\right] \tag{6c}$$

APPENDIX

Derivatives of Rotor Torque Coefficient

The equations for computing the derivatives of the rotor torque coefficient with respect to collective pitch, angle of attack, and $V/\Omega R$ are

$$\frac{\partial C_Q}{\partial A_o} = \frac{\sigma a}{2}\left[\frac{1}{\Omega R}\frac{\partial v_1}{\partial A_o}\left(\frac{1}{4}b_1 - \frac{1}{4}\lambda'\right) - \frac{\partial b_1}{\partial A_o}\left(\frac{1}{4}b_1 + \frac{1}{8}b_1\mu^2 - \frac{1}{4}\lambda'\right) - \frac{1}{3}\lambda\right.$$

$$\left. + \frac{1}{\Omega R}\frac{\partial v}{\partial A_o}\left(\frac{1}{3}A_o + \lambda + \frac{1}{2}a_1\mu\right) - \frac{\partial a_1}{\partial A_o}\left(\frac{1}{2}\mu\lambda + \frac{1}{4}a_1 + \frac{3}{8}a_1\mu^2\right)\right] \qquad (7a)$$

$$\frac{\partial C_Q}{\partial \alpha} = \frac{\sigma a}{2}\left\{\mu\left(\frac{v}{\Omega R} - \frac{1}{3}A_o\right) - \mu^2\left(\frac{1}{2}\frac{\bar{c}_{d,o}}{a} + 1 - \frac{3}{8}a_1^2 - \frac{1}{8}b_1^2 - \frac{1}{2}a_1\tan\alpha\right)\tan\alpha\right.$$

$$- \frac{1}{2}a_1\mu^2 - \frac{a_1 v\mu}{2\Omega R}\tan\alpha + \frac{1}{\Omega R}\frac{\partial v}{\partial \alpha}\left(\frac{1}{3}A_o + \lambda + \frac{1}{2}a_1\mu\right) + \frac{\partial a_1}{\partial \alpha}\left[\frac{\mu v}{2\Omega R} - a_1\left(\frac{1}{4} + \frac{3}{8}\mu^2\right)\right.$$

$$\left.\left. - \frac{1}{2}\mu^2\tan\alpha\right] + \frac{\partial b_1}{\partial \alpha}\left[\frac{1}{4}\lambda' - b_1\left(\frac{1}{4} + \frac{1}{8}\mu^2\right)\right] + \frac{1}{\Omega R}\frac{\partial v_1}{\partial \alpha}\left(\frac{1}{4}b_1 - \frac{1}{4}\lambda'\right)\right\} \qquad (7b)$$

$$\frac{\partial C_Q}{\partial\left(\frac{V}{\Omega R}\right)} = \frac{\sigma a}{2}\left\{\mu\left(\frac{\bar{c}_{d,o}}{a} - \frac{3}{4}a_1^2 - \frac{1}{4}b_1^2\right)\cos\alpha - \left(\frac{1}{3}A_o + \lambda + a_1\mu\right)\sin\alpha\right.$$

$$+ \frac{a_1 v}{2\Omega R}\cos\alpha + \frac{\partial v}{\partial V}\left(\frac{A_o}{3} + \lambda + \frac{a_1\mu}{2}\right) - \frac{\partial a_1}{\partial\left(\frac{V}{\Omega R}\right)}\left[a_1\left(\frac{1}{4} + \frac{3}{8}\mu^2\right) + \frac{\mu\lambda}{2}\right]$$

$$\left. + \frac{\partial b_1}{\partial\left(\frac{V}{\Omega R}\right)}\left[\frac{\lambda'}{4} - \frac{b_1}{4}\left(1 + \frac{1}{2}\mu^2\right)\right] + \frac{\partial v_1}{\partial V}\left(\frac{b_1}{4} - \frac{\lambda'}{4}\right)\right\} \qquad (7c)$$

APPENDIX

Derivatives of Resultant-Force Vector Angle

The equations for computing the derivatives of the resultant-force vector angle a' with respect to collective pitch, angle of attack, and $V/\Omega R$ are

$$\frac{\partial a'}{\partial A_o} = \left(\frac{\partial C_H}{\partial A_o} - \frac{\partial C_T}{\partial A_o} \tan a' \right) \frac{\cos^2 a'}{C_T} \tag{8a}$$

$$\frac{\partial a'}{\partial \alpha} = \left(\frac{\partial C_H}{\partial \alpha} - \frac{\partial C_T}{\partial \alpha} \tan a' \right) \frac{\cos^2 a'}{C_T} \tag{8b}$$

$$\frac{\partial a'}{\partial \left(\frac{V}{\Omega R} \right)} = \left[\frac{\partial C_H}{\partial \left(\frac{V}{\Omega R} \right)} - \frac{\partial C_T}{\partial \left(\frac{V}{\Omega R} \right)} \tan a' \right] \frac{\cos^2 a'}{C_T} \tag{8c}$$

REFERENCES

1. Anon.: Helicopter Flying and Ground Handling Qualities; General Requirements for Military Specification MIL-H-8501A, Sept. 7, 1961, Amendment 1, Apr. 3, 1962.

2. Heyson, Harry H.: Linearized Theory of Wind-Tunnel Jet-Boundary Corrections and Ground Effect for VTOL-STOL Aircraft. NASA TR R-124, 1962.

3. Gessow, Alfred; and Myers, Garry C., Jr.: Aerodynamics of the Helicopter. The Macmillan Co., c.1952.

4. Coleman, Robert P.; Feingold, Arnold M.; and Stempin, Carl W.: Evaluation of the Induced-Velocity Field of an Idealized Helicopter Rotor. NACA WR L-126, 1945. (Formerly NACA ARR L5E10.)

5. Gessow, Alfred; and Crim, Almer D.: A Method for Studying the Transient Blade-Flapping Behavior of Lifting Rotors at Extreme Operating Conditions. NACA TN 3366, 1955.

6. Sweet, George E.: Static-Stability Measurements of a Stand-On Type Helicopter With Rigid Blades, Including a Comparison With Theory. NASA TN D-189, 1960.

7. Connor, Andrew B.; and Tapscott, Robert J.: A Flying-Qualities Study of a Small Ram-Jet Helicopter. NASA TN D-186, 1960.

8. Schuck, George I.: An Analysis of Results From Army-Sponsored VTOL Research Aircraft. TREC Tech. Rept. 61-3, U.S. Army Transportation Res. Command (Fort Eustis, Va.), Jan. 1961.

9. Gustafson, F. B.; and Tapscott, Robert J.: Methods for Obtaining Desired Helicopter Stability Characteristics and Procedures for Stability Predictions. NACA Rep. 1350, 1958. (Supersedes NACA TN 3945.)

10. Heyson, Harry H.: Preliminary Results From Flow-Field Measurements Around Single and Tandem Rotors in the Langley Full-Scale Tunnel. NACA TN 3242, 1954.

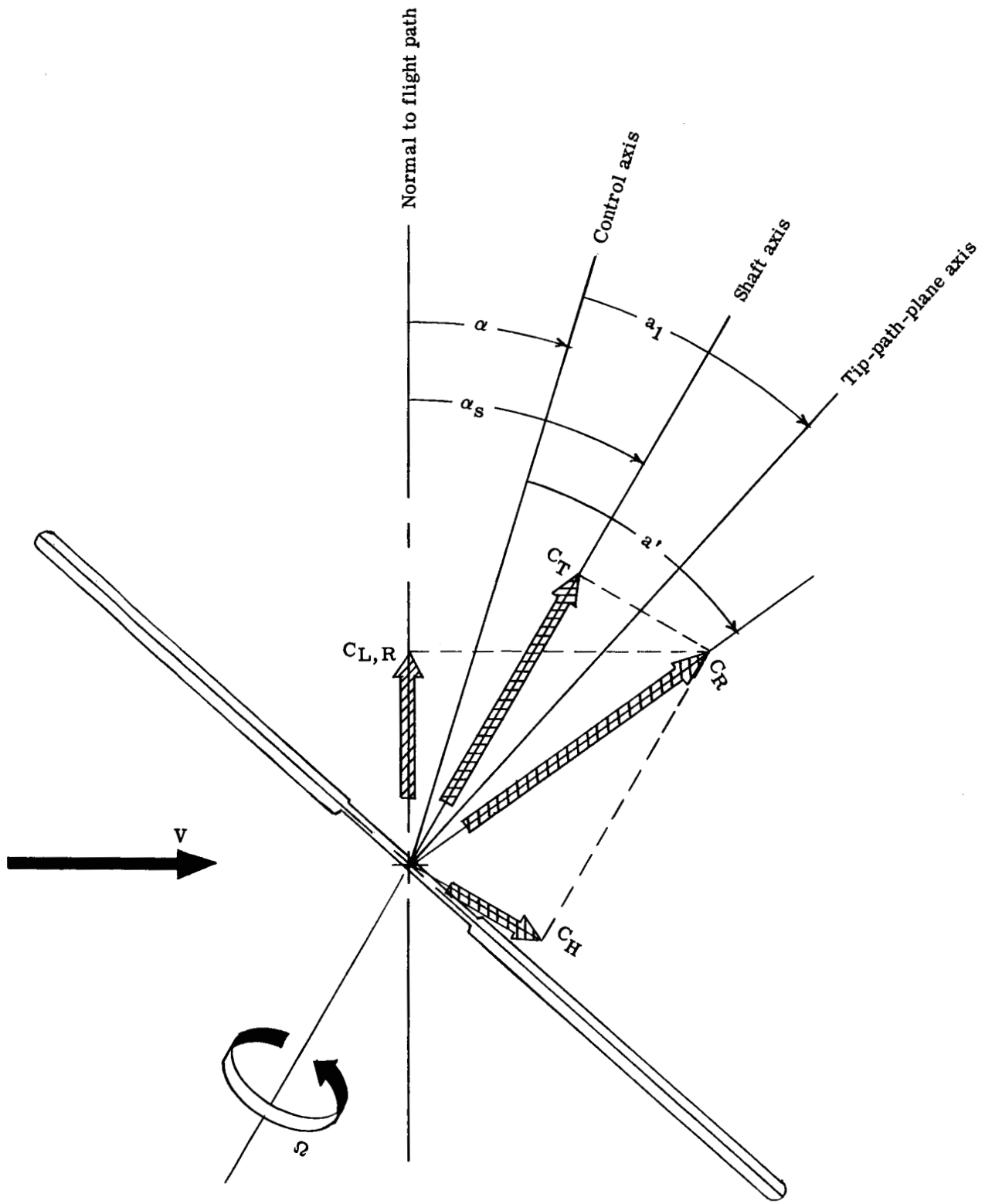

Figure 1.- Notation showing positive directions of forces and angles.

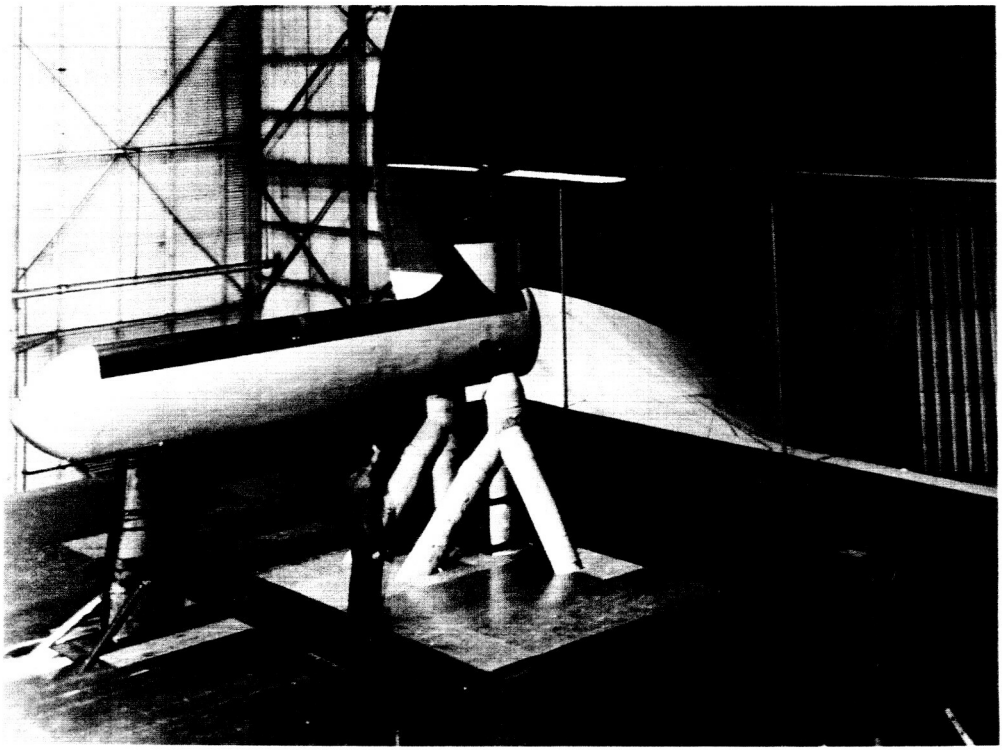

L-62-3093

Figure 2.- General view of 15-foot-diameter rotor installed in Langley full-scale tunnel.

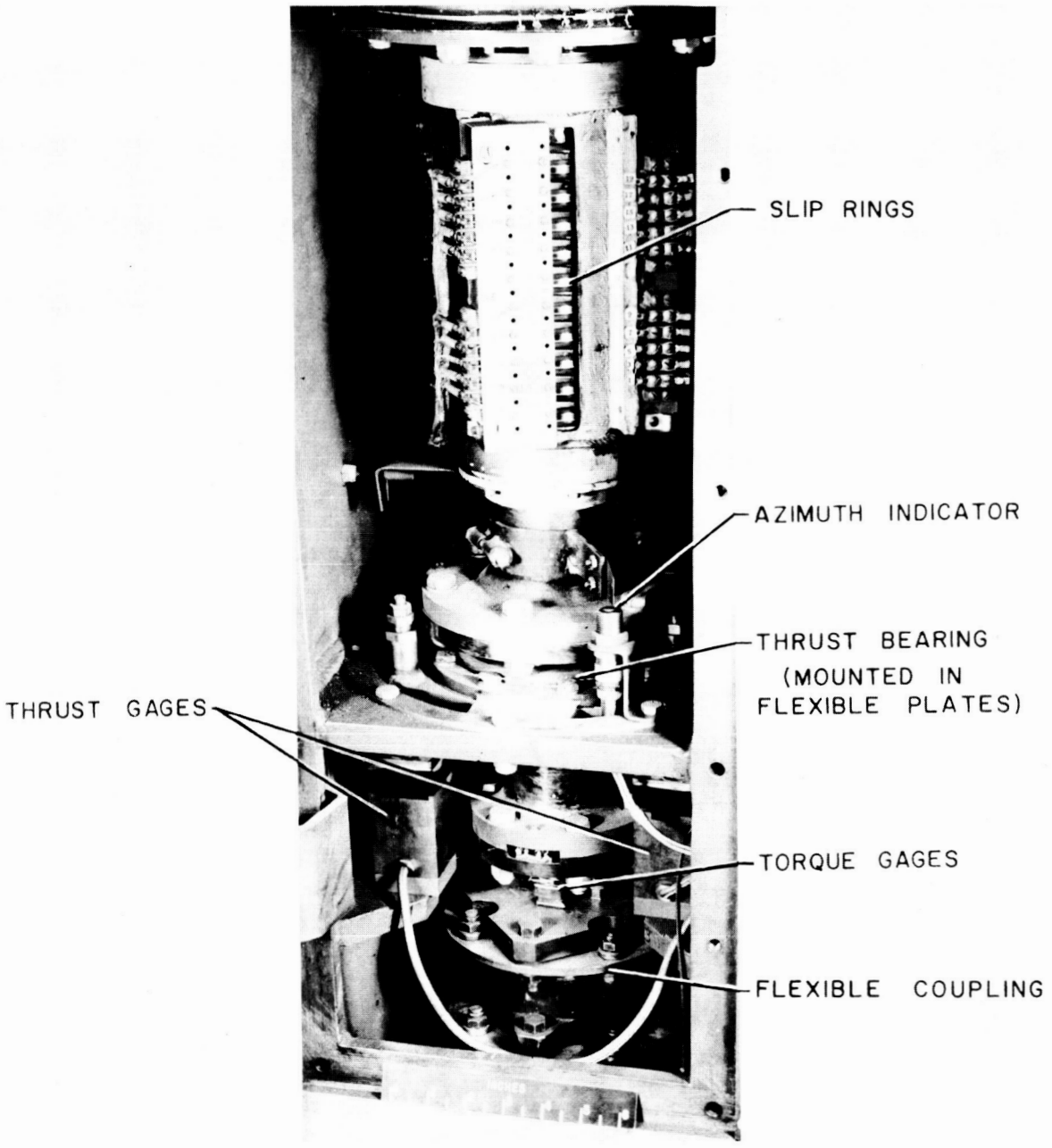

Figure 3.- Force measuring system. L-58-621a.1

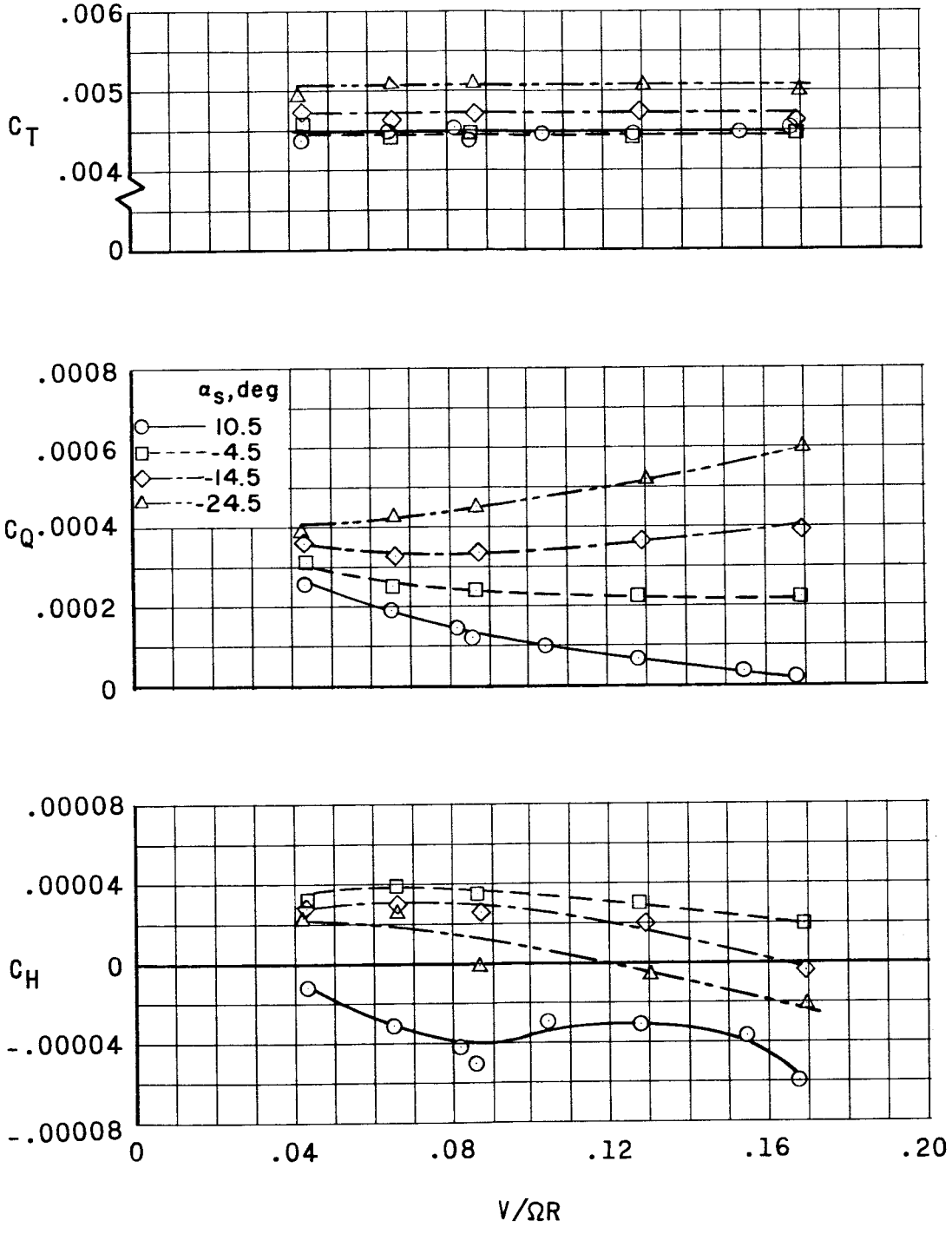

Figure 4.- Variation of rotor characteristics with tip-speed ratio for a constant rotor lift, $C_{L,R} = 0.0045$.

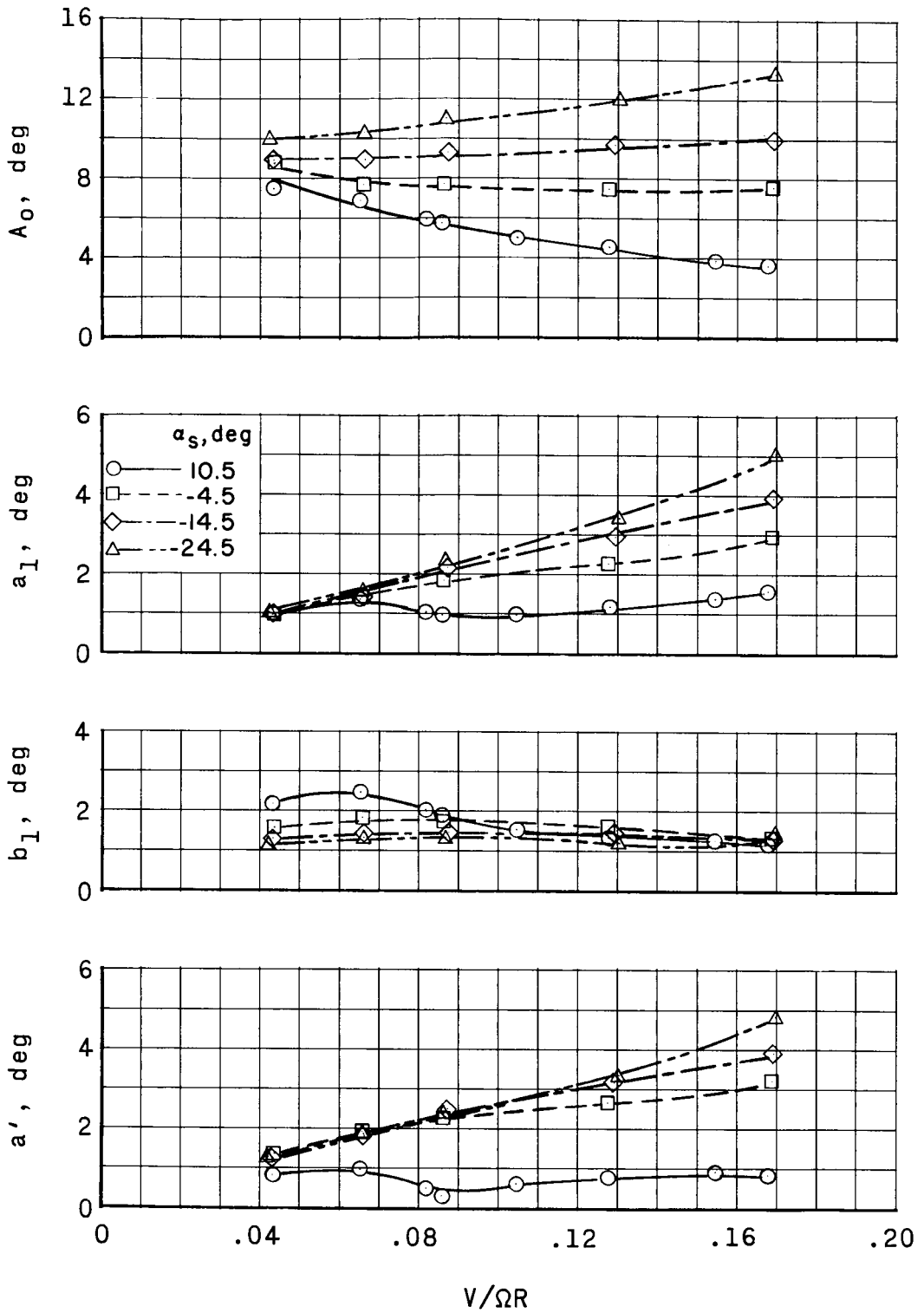

Figure 4.- Concluded.

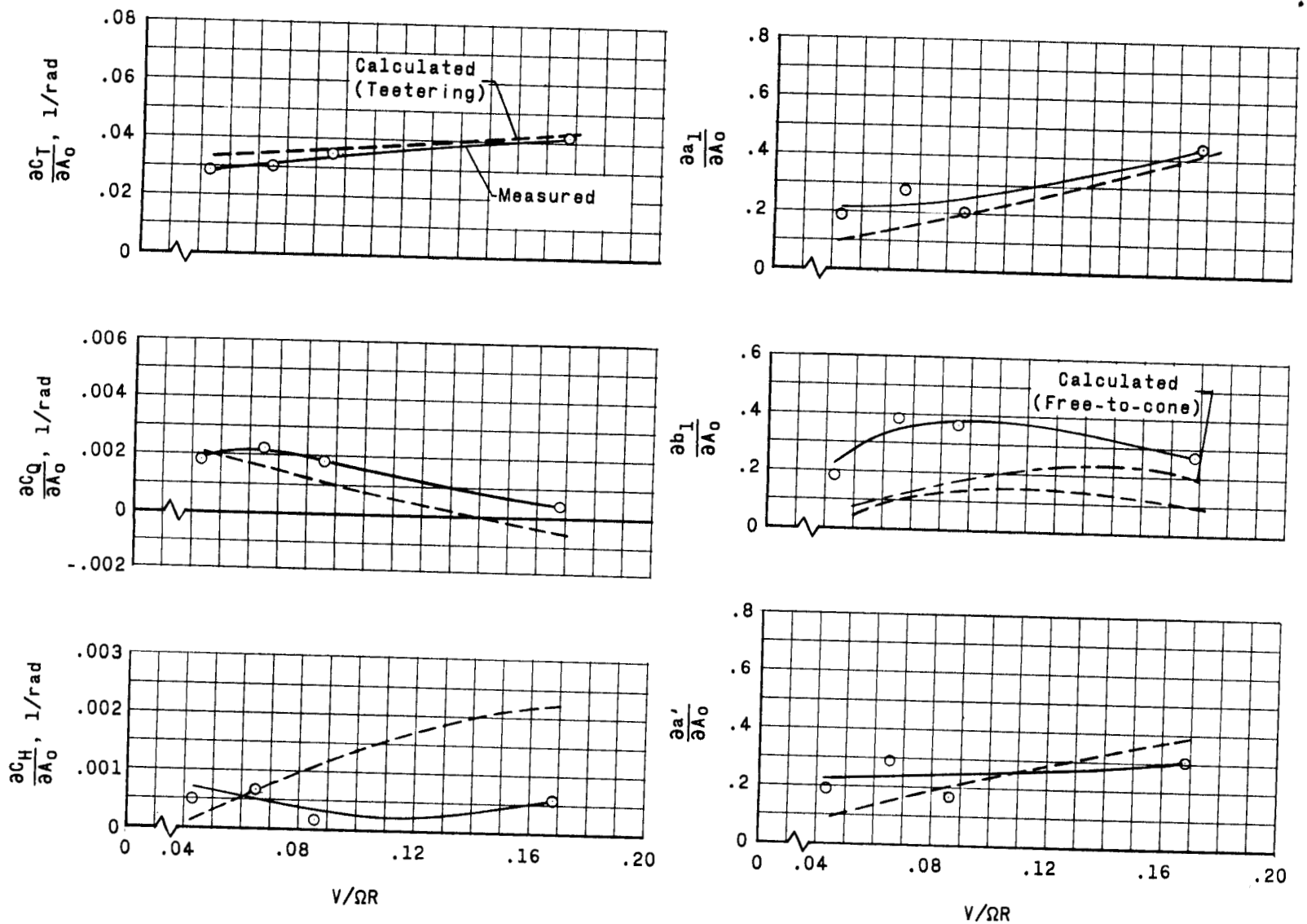

(a) $\alpha_s = 10.5°$.

Figure 5.- Comparison between measured and calculated rotor stability derivatives with respect to collective pitch.

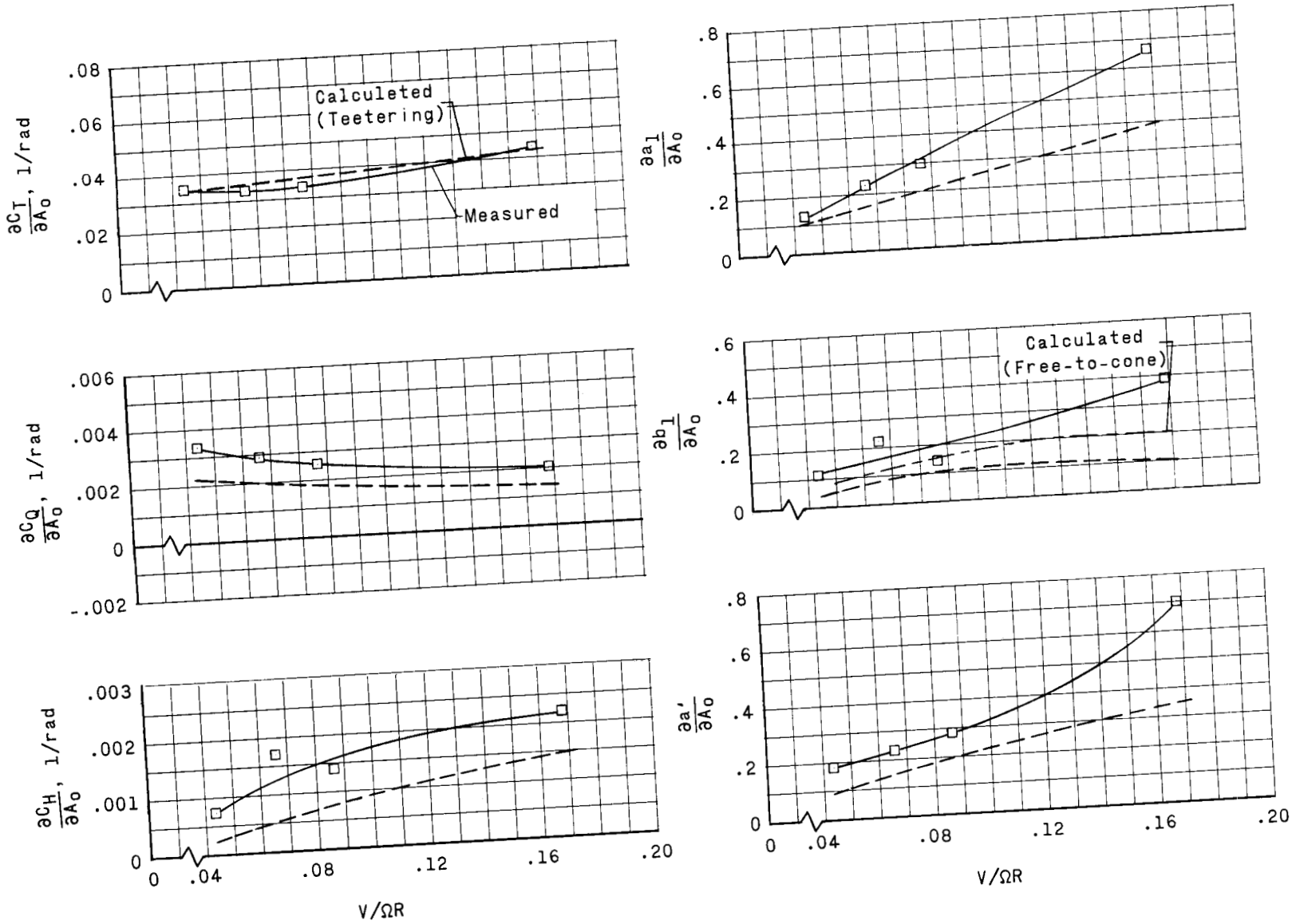

(b) $\alpha_s = -4.5^o$.

Figure 5.- Continued.

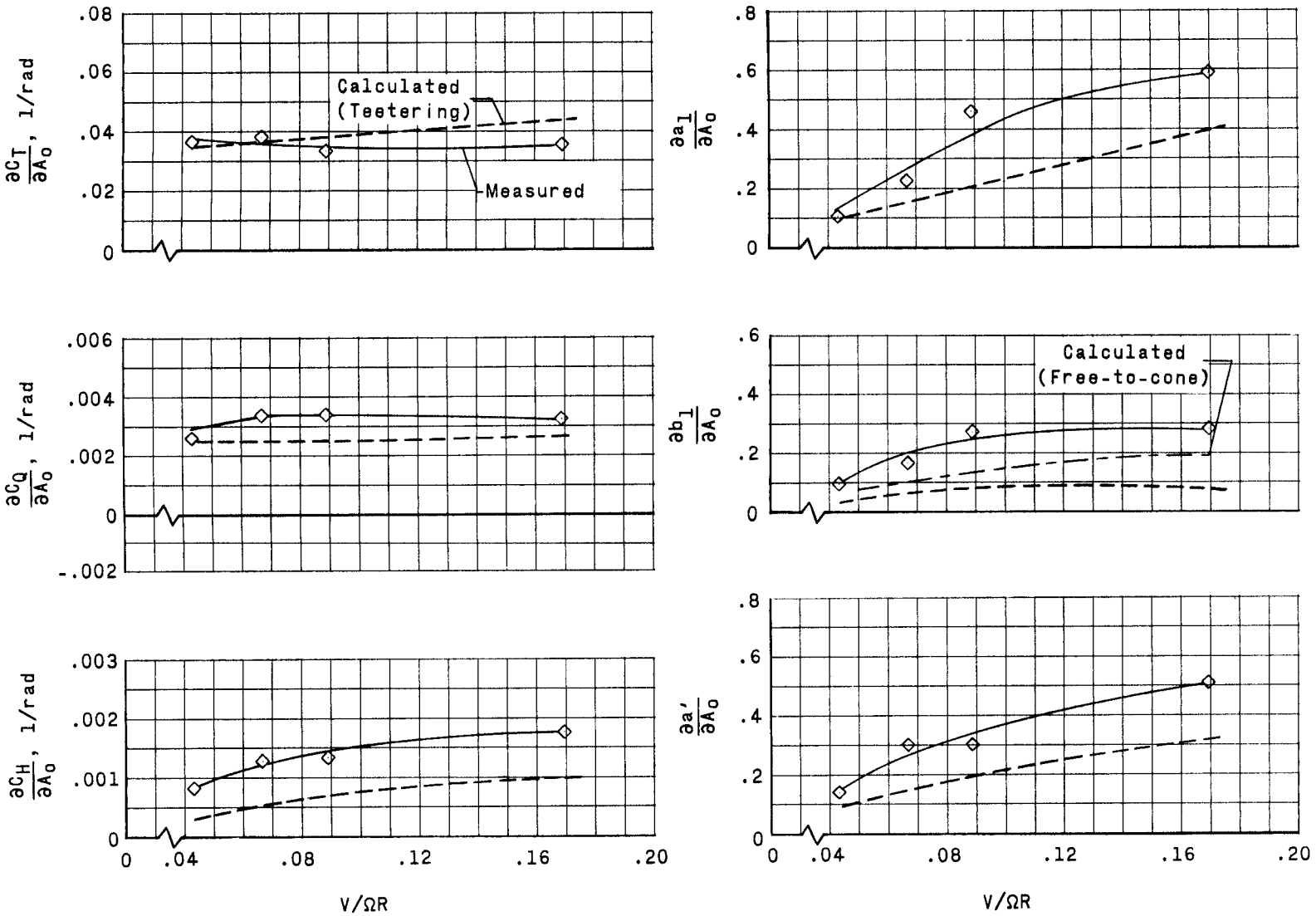

(c) $\alpha_s = -14.5^\circ$.

Figure 5.- Continued.

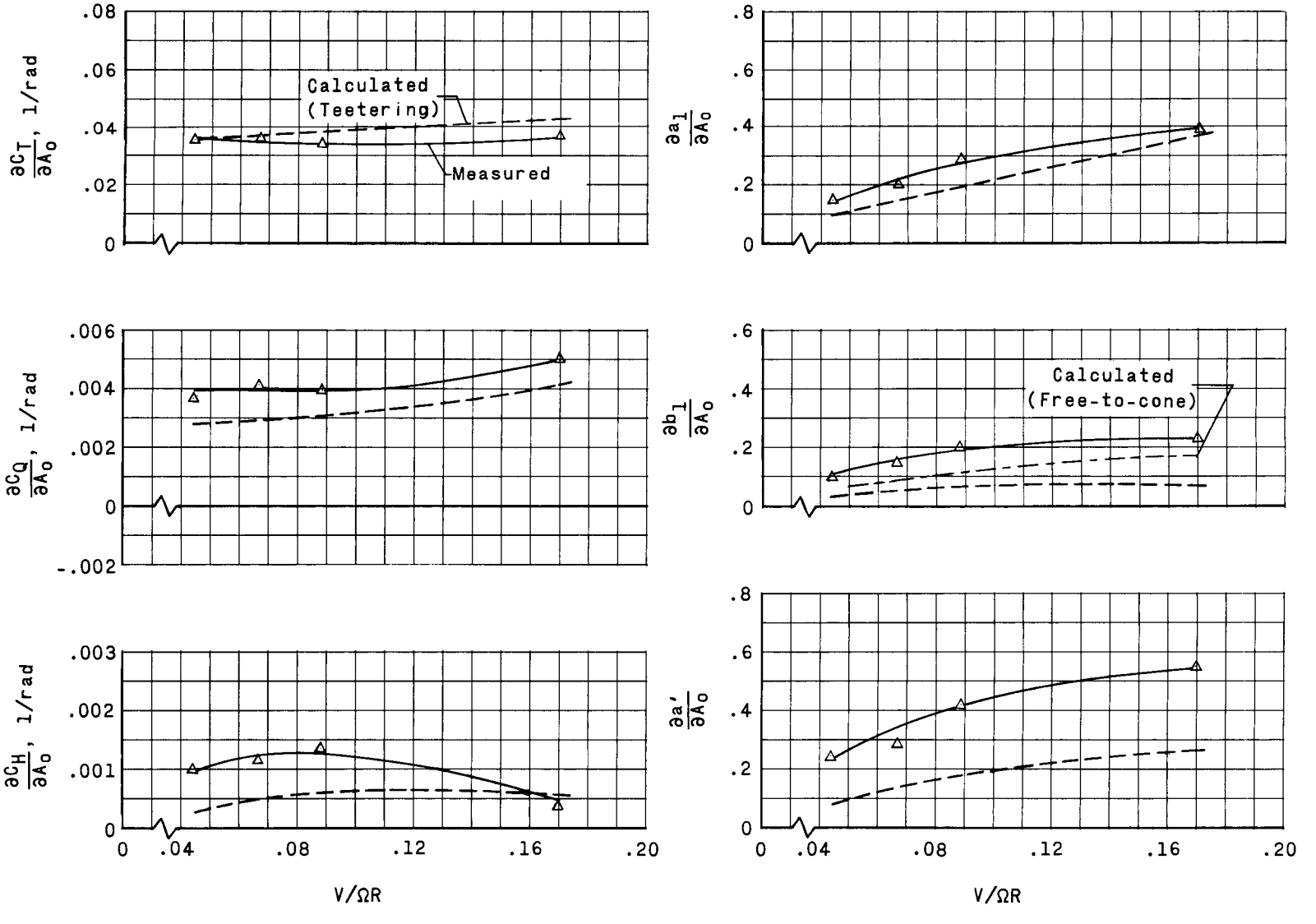

(d) $\alpha_s = -24.5^\circ$.

Figure 5.- Concluded.

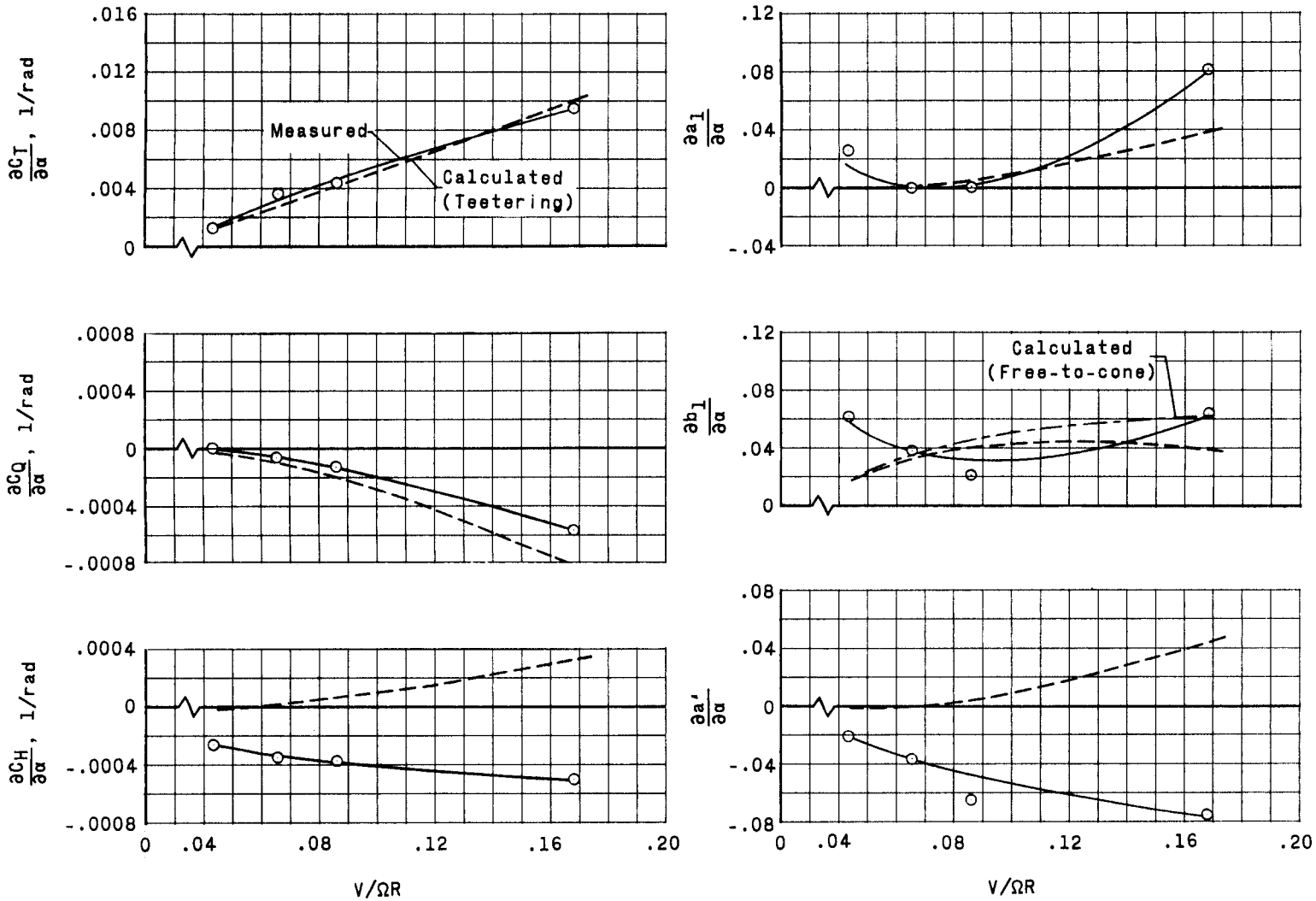

(a) $\alpha_s = 10.5°$.

Figure 6.- Comparison between measured and calculated rotor stability derivatives with respect to angle of attack.

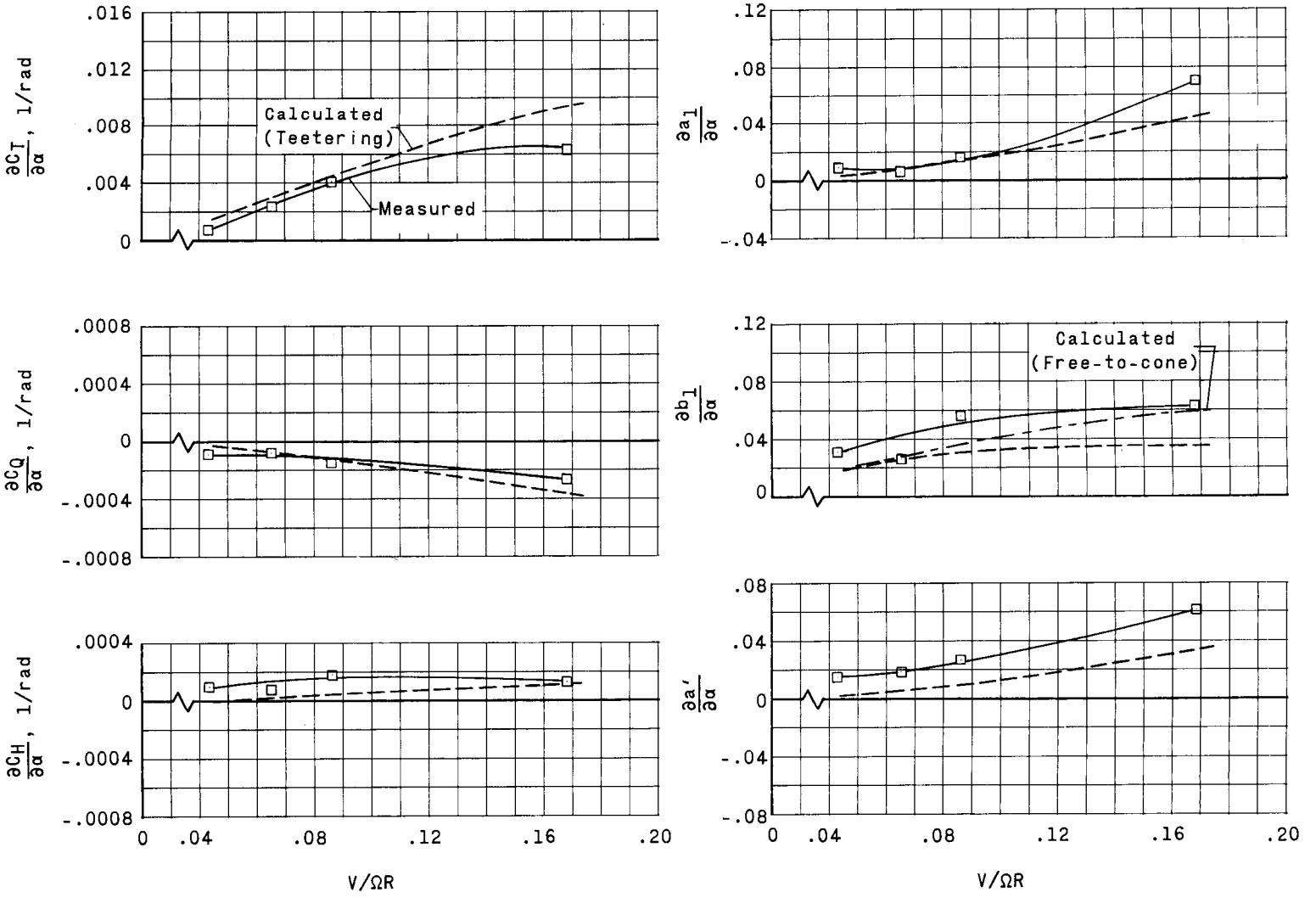

(b) $\alpha_s = -4.5^\circ$.

Figure 6.- Continued.

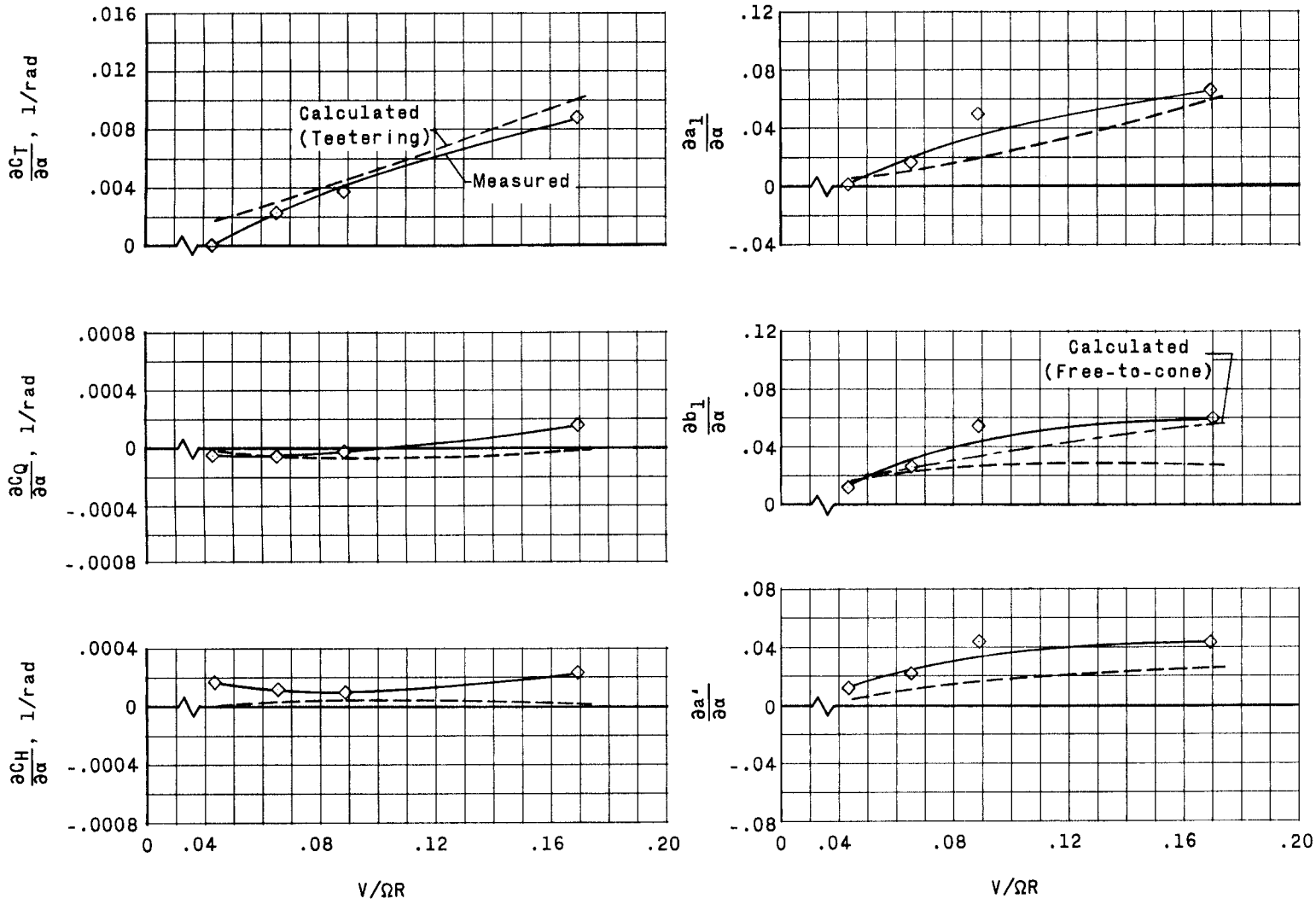

(c) $\alpha_s = -14.5^\circ$.

Figure 6.- Continued.

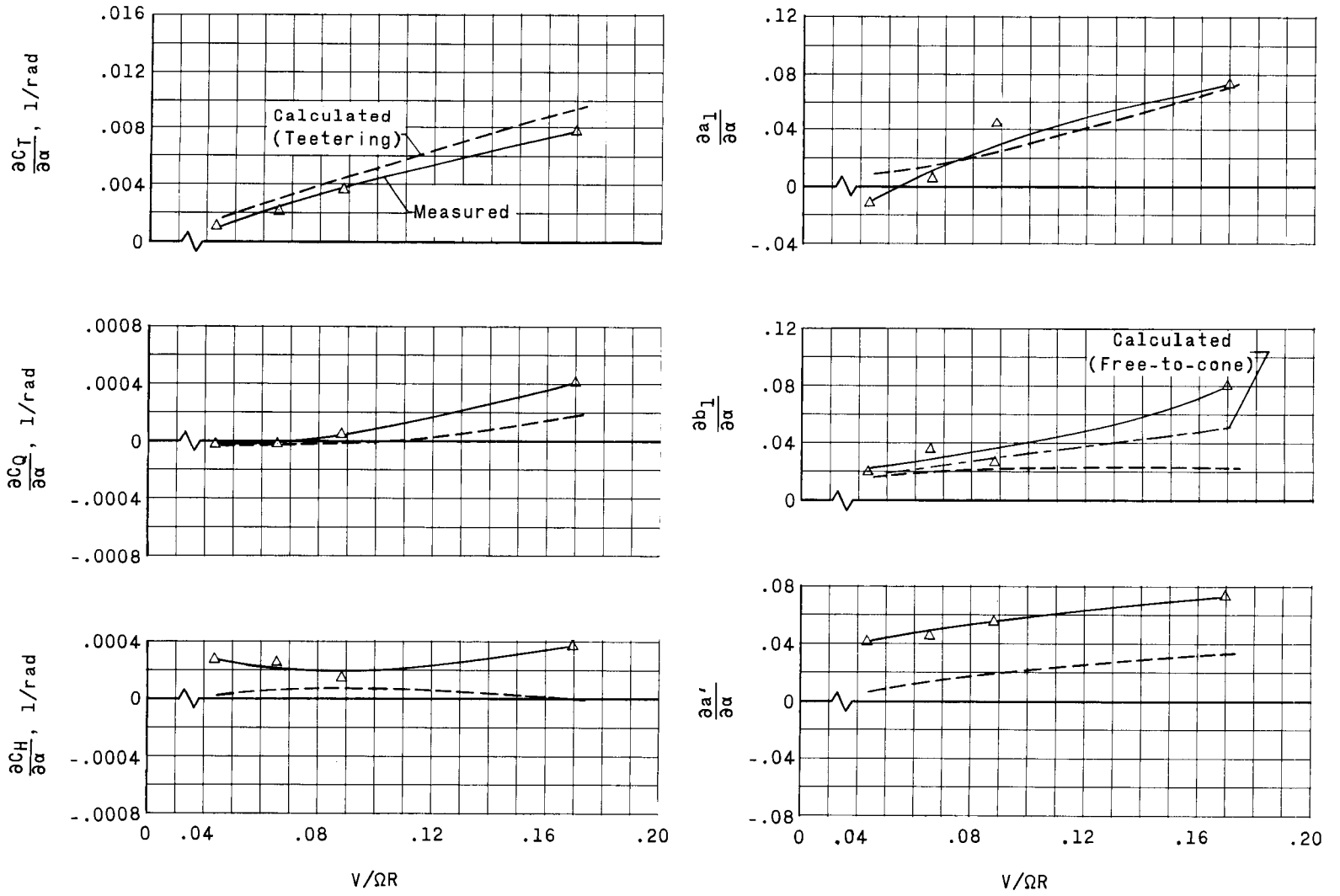

(d) $\alpha_s = -24.5^\circ$.

Figure 6.- Concluded.

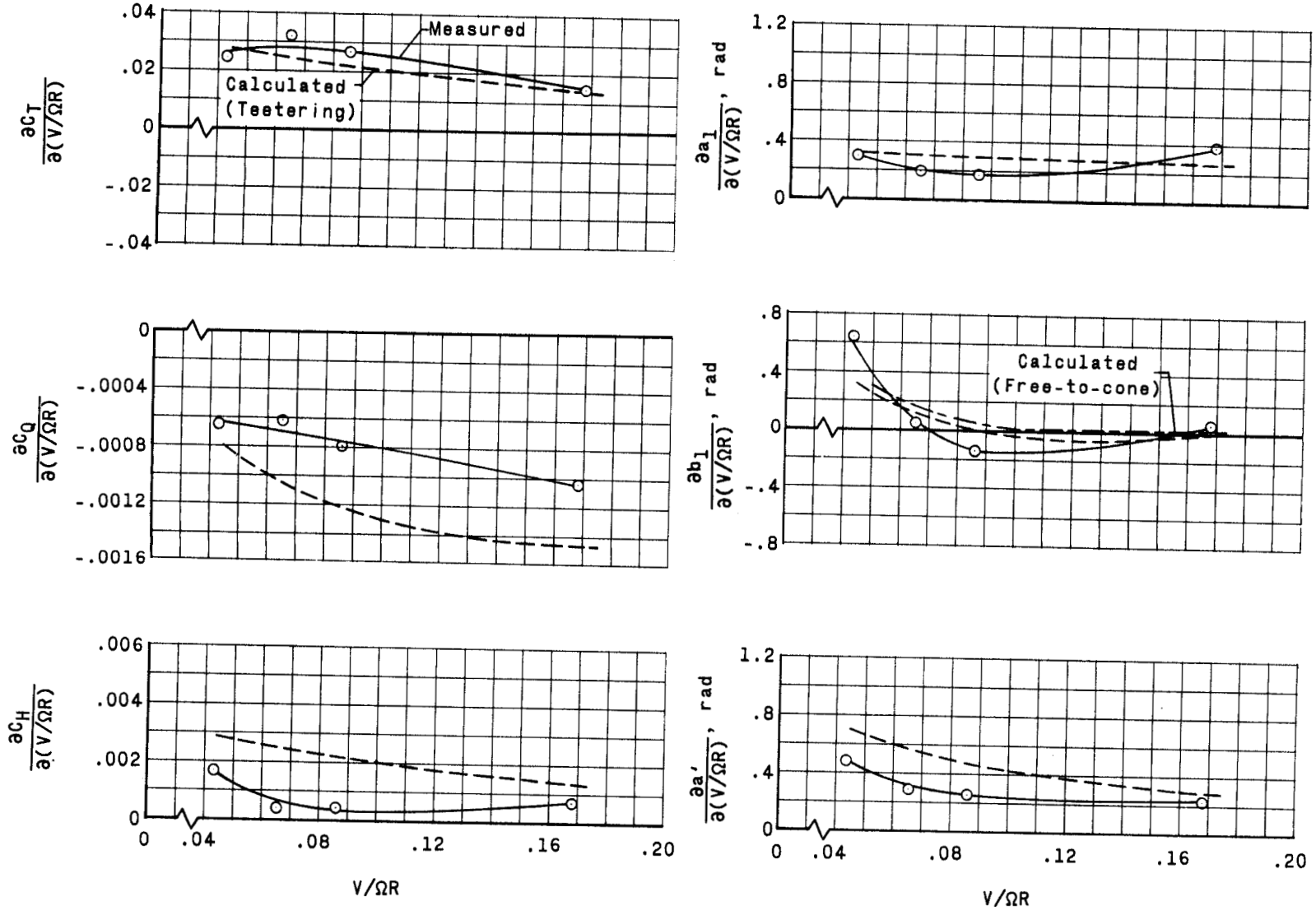

(a) $\alpha_s = 10.5°$.

Figure 7.- Comparison between measured and calculated rotor stability derivatives with respect to tip-speed ratio.

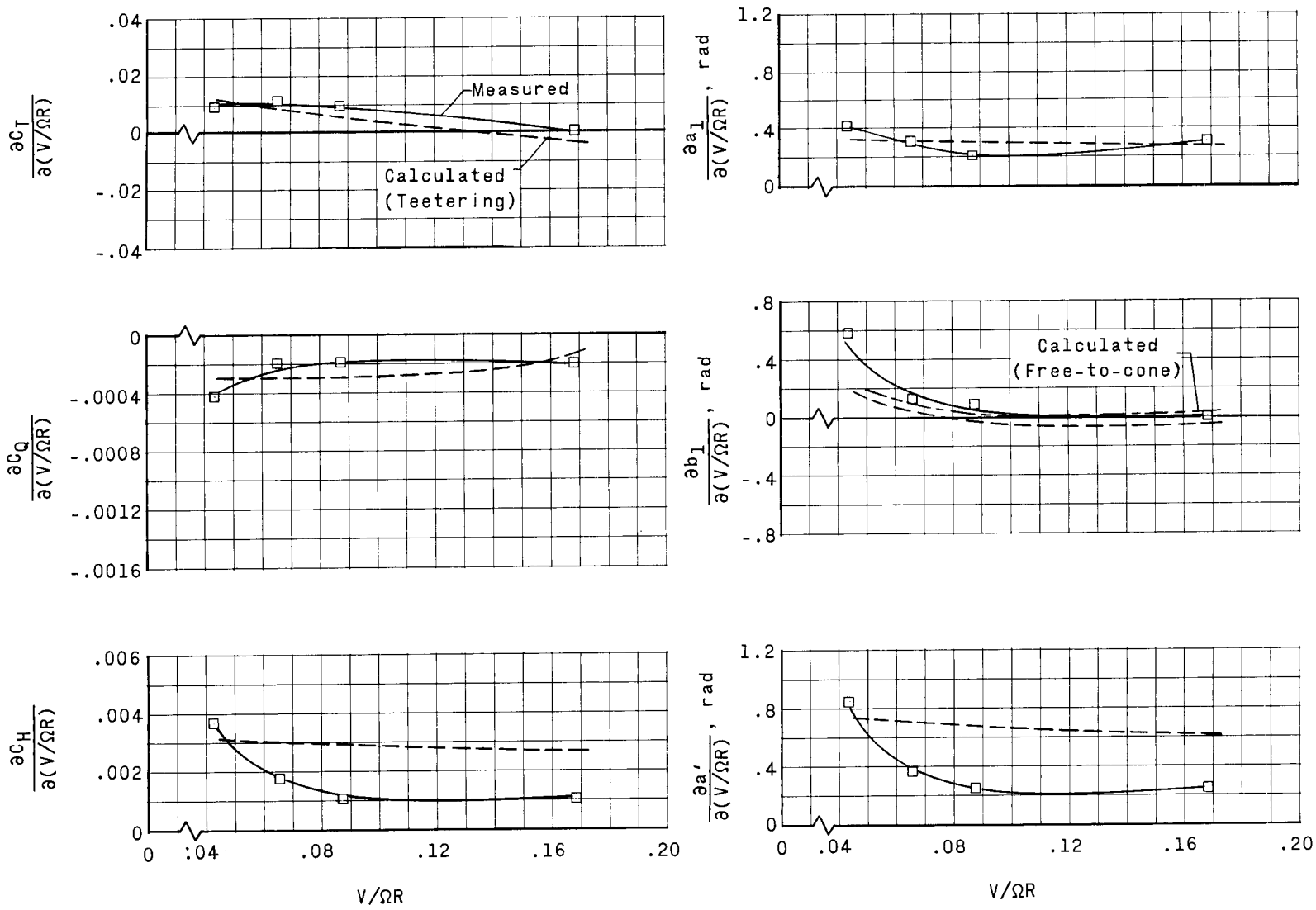

(b) $\alpha_s = -4.5^\circ$.

Figure 7.- Continued.

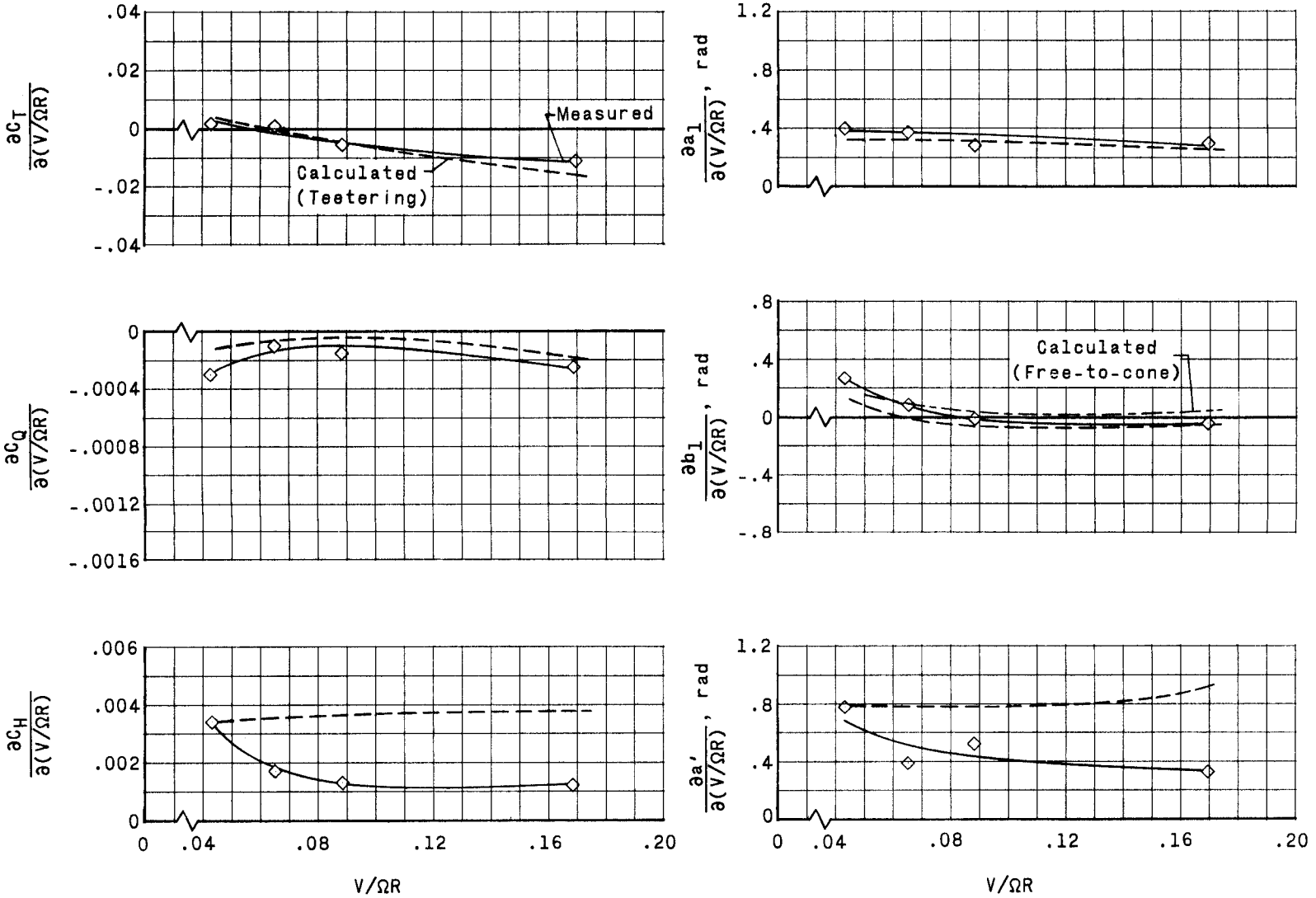

(c) $\alpha_s = -14.5^\circ$.

Figure 7.- Continued.

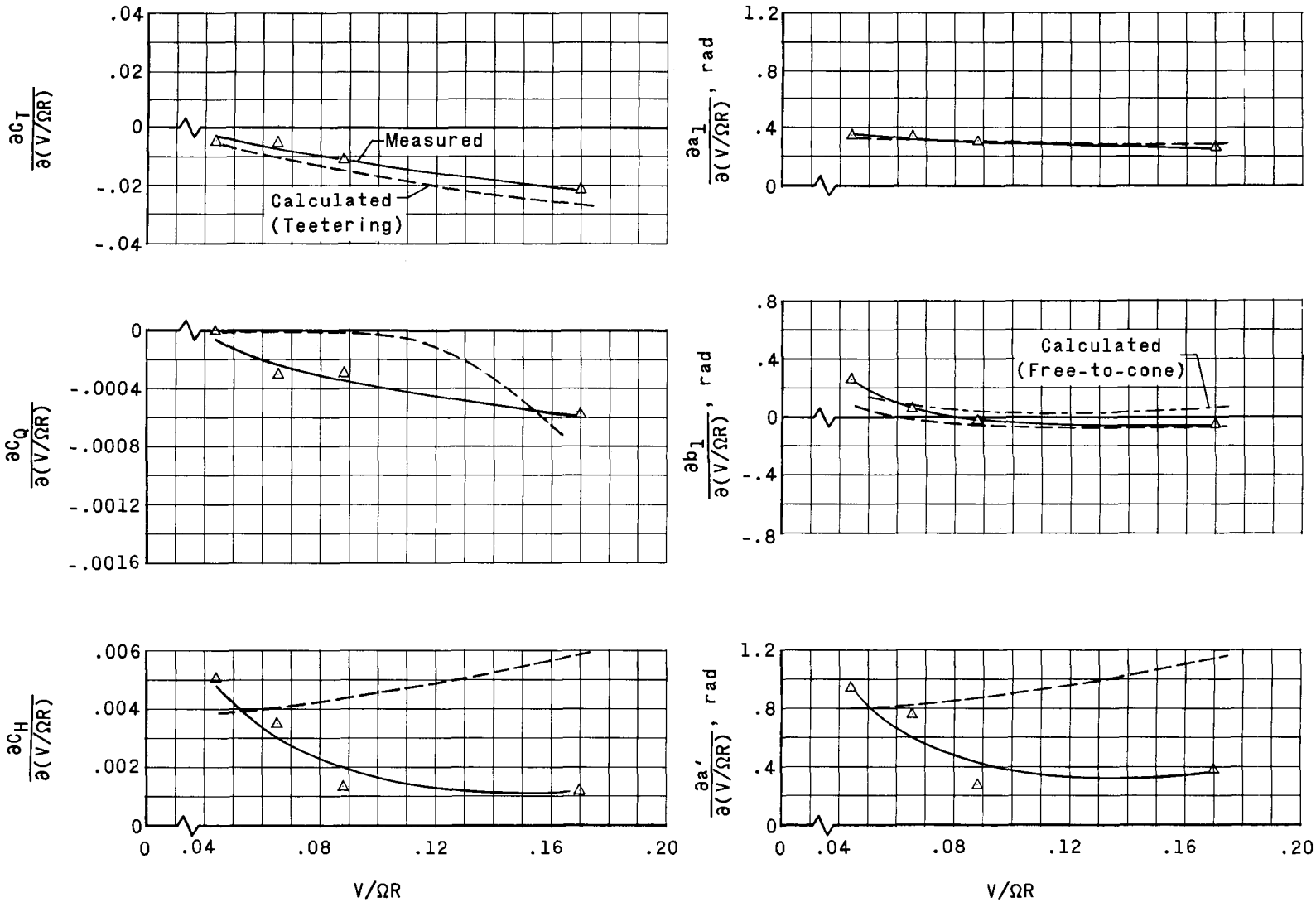

(d) $\alpha_s = -24.5^\circ$.

Figure 7.- Concluded.

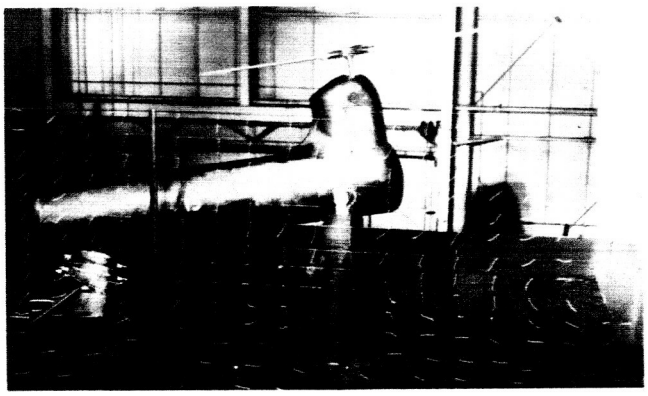

(a) $\alpha_s = 10.5^\circ$.

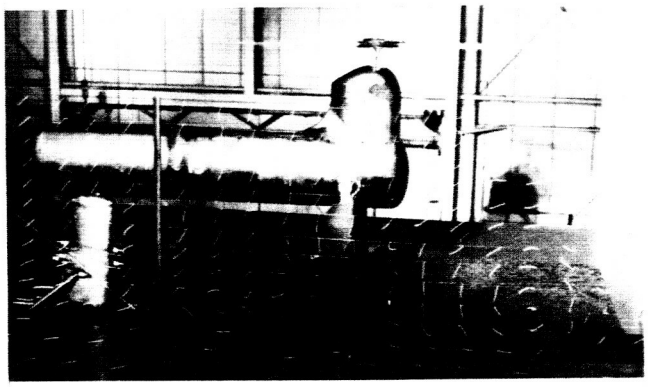

(b) $\alpha_s = 0.5^\circ$.

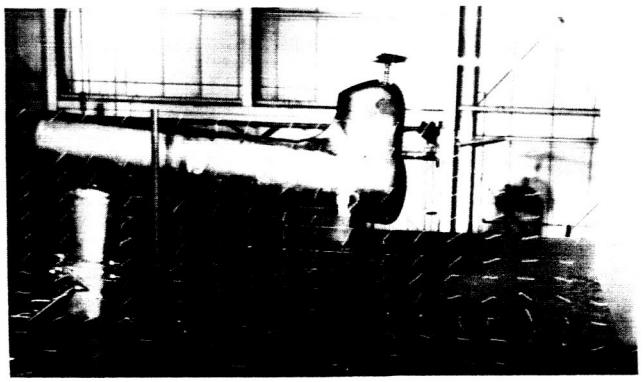

(c) $\alpha_s = -4.5^\circ$.

L-64-10201

Figure 8.- Variation of wake pattern at various angles of attack for a constant rotor lift, $C_{L,R} = 0.0045$. $V/\Omega R = 0.032$.

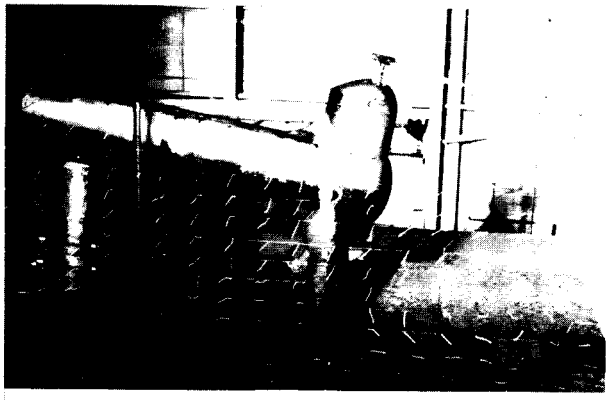

(d) $\alpha_s = -9.5°$.

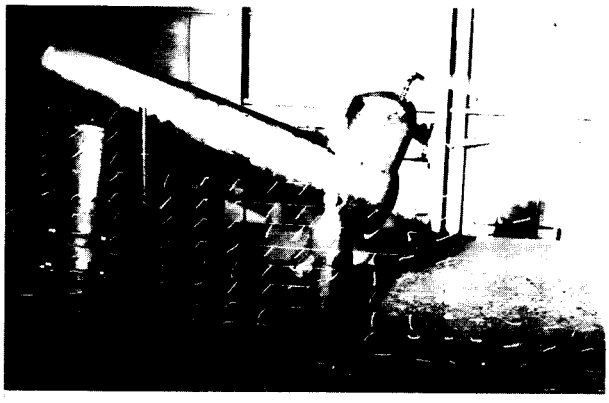

(e) $\alpha_s = -19.5°$.

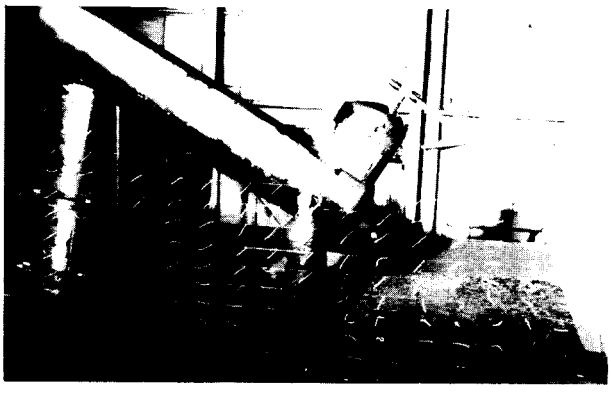

(f) $\alpha_s = -29.5°$.

Figure 8.- Concluded. L-64-10202

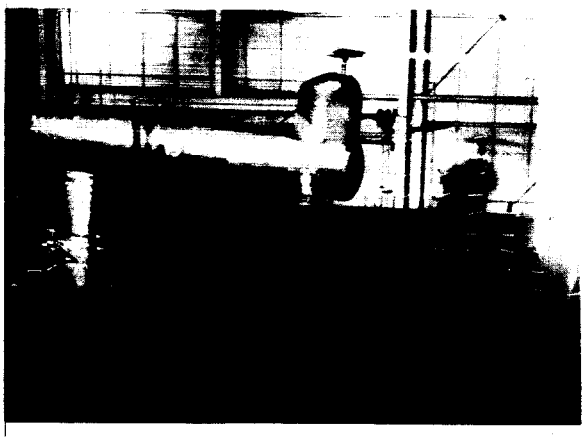

$V/\Omega R = 0.032$

$V/\Omega R = 0.043$

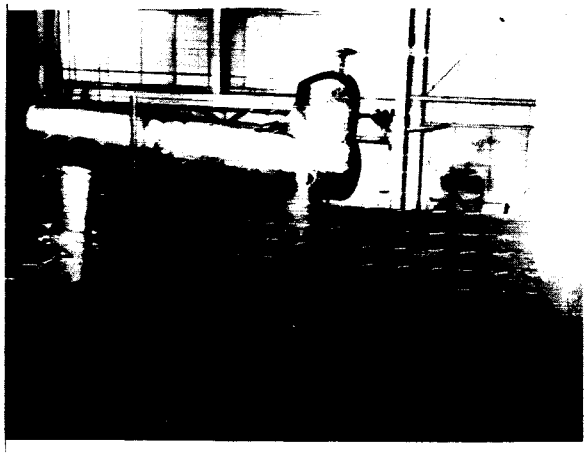

$V/\Omega R = 0.064$

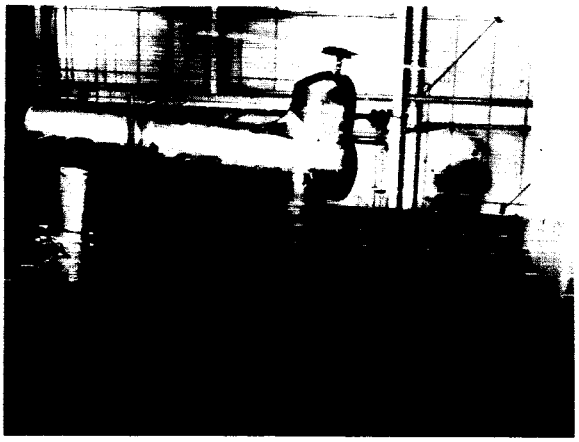

$V/\Omega R = 0.086$

(a) $\alpha_s = -4.5^\circ$.

L-64-10203

Figure 9.- Variation of wake pattern at various tip-speed ratios for a constant rotor lift, $C_{L,R} = 0.0045$.

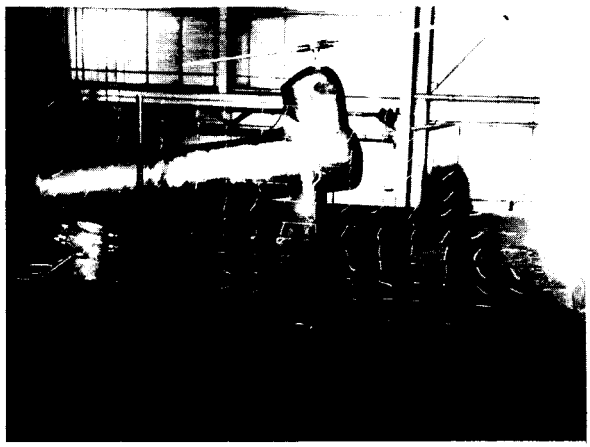

$V/\Omega R = 0.032$

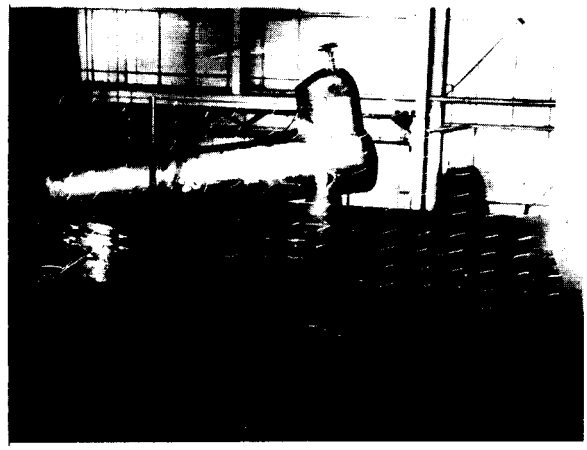

$V/\Omega R = 0.043$

$V/\Omega R = 0.064$

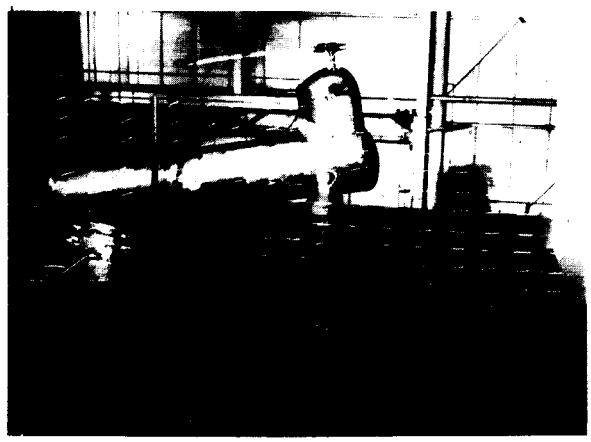

$V/\Omega R = 0.086$

(b) $\alpha_s = 10.5^\circ$.

Figure 9.- Concluded. L-64-10204

NASA-Langley, 1965 L-4217